Measurement of the piezoelectric tensor of an organic crystal by the x-ray method: The nonlinear optical crystal 2-methyl 4-nitroaniline

Antoine Paturle,*,† Heinz Graafsma, H.-S. Sheu,‡ and Philip Coppens†
Department of Chemistry, State University of New York at Buffalo, Buffalo, New York 14214

Pierre Becker
Laboratoire de Cristallographie, Centre National de la Recherche Scientifique, 25 avenue des Martyrs, 38000 Grenoble, France
(Received 22 October 1990)

The piezoelectric tensor of the organic nonlinear optical compound 2-methyl 4-nitroaniline (MNA) is refined from the measurements of the shift of the Bragg peaks on application of an external electric field. The "three-step modulation" method is used, in which the gating of the x-ray signal is synchronized with the variation of the electric field. The piezoelectric tensor is dominated by one coefficient, $|d_{11}| = 13.8(1) \times 10^{-12}$ C/N, which is, to our knowledge, the largest ever observed in an organic molecular crystal and six times greater than the largest coefficient of α quartz. Here, the x axis is chosen along the polar axis of the crystal. The large linear electro-optical effect observed in MNA is reinterpreted in terms of the piezoelectric-photoelastic effect.

INTRODUCTION

Though the macroscopic theory of the piezoelectric effect has been extensively developed, there is a general lack of insight at the atomic level. With the more powerful x-ray sources now available, and developments in electronics, it has become possible to study the response of crystals to an external field from the changes in the diffraction pattern. We describe here such a study of the converse piezoelectric effect on the nonlinear optical crystal 2-methyl 4-nitroaniline (MNA).

THE BARSCH EQUATION

When a static or low-frequency electric field is applied to a piezoelectric crystal, strains are developed in the crystal: this is the well-known converse piezoelectric effect. An element of the strain tensor ϵ_{ij} is linearly related to the applied electric field by the expression

$$\epsilon_{ij} = \sum_{k=1}^{3} d_{kij} E_k \ , \tag{1}$$

where E_k is the kth component of the electric field **E**, and d_{kij} is the kijth element of the third-rank piezoelectric tensor d.

The macroscopic deformation of the crystal is due to a microscopic deformation of the unit cell. In the case of an elastic, homogeneous, and infinitesimal deformation, it can be shown[1] that the Bragg angle θ_r of a reflection r will be changed by an amount $\Delta\theta_r$ given by

$$\begin{aligned}\Delta\theta_r &= -\tan\theta_r \sum_{i=1}^{3}\sum_{j=1}^{3} h_{r,i} h_{r,j} \epsilon_{ij} \\ &= -E \tan\theta_r \sum_{k=1}^{3}\sum_{i=1}^{3}\sum_{j=1}^{3} e_k h_{r,i} h_{r,j} d_{kij} \ ,\end{aligned} \tag{2}$$

where the e_k's and the $h_{r,i}$'s are the direction cosines of the electric field (of magnitude E) and the diffraction vector $\mathbf{h}_r$, respectively.

Expression (2) provides the basis for the refinement of the piezoelectric tensor elements d_{ijk} (or the strain tensor elements ϵ_{ij}) from a set of measured values of $\Delta\theta_r$. The change in the unit-cell dimensions can be derived directly from ϵ, as described by Barsch.[1]

THE MEASUREMENT OF THE θ SHIFTS

Typical values for $\Delta\theta$ of $10^{-3}°$–$10^{-4}°$ are comparable with the precision of a good quality diffractometer. Nevertheless, application of the "three-step modulation" method, followed by analysis of the intensity change at each point in a step scan, allows the shift in the profile to be determined with a precision of about $10^{-6}°$.

The "three-step modulation" method

This method[2] has been designed to measure very small variations in the x-ray-diffracted intensities upon application of the external electric field. It is an extension of a method described earlier by Godefroy[3] and Fujimoto.[4]

The method uses a *quasistatic* electric field of square-wave shape and low frequency. The diffraction signal is gated to three different counting chains depending on the direction of the applied field (Fig. 1). The three reflection profiles I_+, I_0, and I_- collected in a single scan of a reflection thus correspond to the three steps in the field variation ("field up," zero field, and "field down").

Similar methods are known in electronics as "synchronous modulation-demodulation" methods: the crystal is modulated at the frequency ν_E of the applied electric field, while the response of the detector is demodulated by electronics synchronized with the modulation. The method effectively eliminates experimental fluctuations of

 ©1991 The American Physical Society

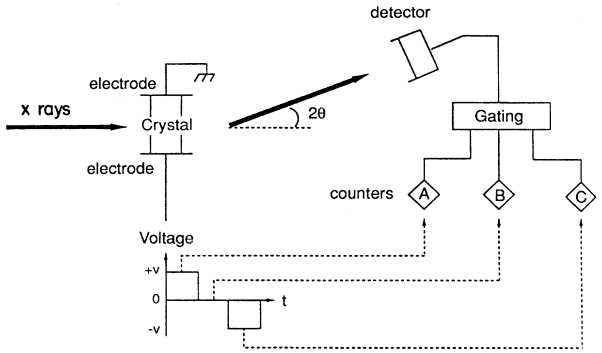

FIG. 1. The three-step modulation method.

frequency different from ν_E. Suitable choice of ν_E and correct treatment of possible systematic errors allow measurement of relative changes in the intensity as small as 10^{-5}–10^{-6}.

The measurement of the shifts $\Delta\theta$

(a) The effect of the electric field on the diffracted profile may be threefold: change in the integrated intensity, change in the Bragg position, and a possible change in the shape of the profile. In MNA and other related organic compounds,[5] the change in the integrated intensity is at most 1%, more often $(10^{-2}$–$10^{-3})$%. No change in the shape of the profile is observed. The 2θ shift of the profile, although small, induces *local* (i.e., at each step of the scan) variations in the intensity of typically 10%. As shown in the Appendix, for small shifts and fixed profile shape, the *local* shift $\Delta 2\theta_i$ at step i of the scanned profile is inversely proportional to the first derivative of the zero-field profile at i, or

$$\Delta 2\theta_{\pm 0,i} = -\eta_{\pm 0,i} \frac{I_0(2\theta_i)}{\dot{I}_0(2\theta_i)} , \tag{3}$$

where the subscript $\pm$ indicates "field up" or "field down," and $\eta_{\pm 0,i}$ are the "response ratios" defined as

$$\eta_{\pm,i} = \frac{\Delta I_{\pm,i}}{I_0(2\theta_i)} = \frac{I_{\pm}(2\theta_i) - I_0(2\theta_i)}{I_0(2\theta_i)}$$

and

$$\dot{I}_0(2\theta_i) = \left[\frac{\partial I_0}{\partial 2\theta} \right]_{2\theta = 2\theta_i} .$$

From the experimental $\Delta I_{\pm,i}$ and numerically computed derivatives of I_0, $\Delta\theta_{\pm,i}$ can be evaluated at each point of the scan.

(b) For a constant shape of the profile, the shifts $\Delta 2\theta_{\pm 0,i}$'s should be equal at each point of the scan, as the whole profile is shifted. As a result of measurement errors, the $\Delta 2\theta_{\pm 0,i}$'s follow a distribution that is approximately Gaussian (Fig. 2). The mean of this distribution $\langle \Delta 2\theta_{\pm 0} \rangle$ will be the best estimate of $\Delta 2\theta_{\pm 0}$:

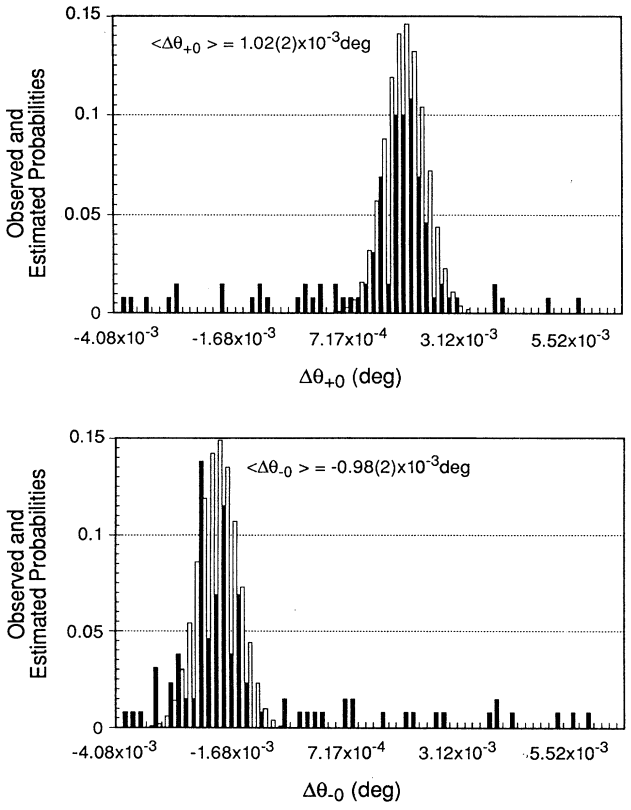

FIG. 2. Observed (black) and estimated Gaussian (white) probability distributions of $\Delta\theta_{+0}$ and $\Delta\theta_{-0}$ for the $(1\,-1\,2)$ reflection with a field of 2.5×10^6 V/m directed along the polar axis. The mean values are $\langle \Delta\theta_{+0} \rangle = -2.50(7)\times 10^{-4}$° and $\langle \Delta\theta_{-0} \rangle = 2.33(7)\times 10^{-4}$°.

$$\langle \Delta 2\theta_{\pm,0} \rangle = \frac{\sum_{i=1}^{N} \frac{\Delta 2\theta_{\pm 0,i}}{\sigma^2(\Delta 2\theta_{\pm 0,i})}}{\sum_{i=1}^{N} \frac{1}{\sigma^2(\Delta 2\theta_{\pm 0,i})}} , \tag{4a}$$

its variance being

$$\sigma^2 \langle \Delta 2\theta_{\pm 0} \rangle = \frac{1}{\sum_{i=1}^{N} \frac{1}{\sigma^2(\Delta 2\theta_{\pm 0,i})}} , \tag{4b}$$

where $\sigma(\Delta 2\theta_{\pm 0,i})$ is the standard deviation of the measured $\Delta 2\theta_{\pm 0,i}$. N is about 130 in the experiments reported here.

APPLICATION TO 2-METHYL 4-NITROANILINE

A large body of both theoretical and experimental results for 2-methyl 4-nitroaniline has been accumulated. Though the crystals have one of the largest known second-harmonic generation coefficients,[6] practical applications have been limited to thin films because of the absence of a phase-matching angle in bulk crystals.[7] MNA

also has an exceptionally large dc linear electro-optic effect.[8-10]

Description of the structure

A main feature of the nitroanilines is their electron donor-acceptor character. In MNA (Fig. 3), charge transfer of about $0.3e$ between the amino NH_2 donor group and the nitro NO_2 acceptor group at the opposite ends of the highly polarizable aromatic ring induces a dipole moment with an observed value of 6.2 D.[11] Our calculations with the program HONDO,[12] and a 6-31G basis set give a value of 8.65 D. They show the dipole moment to be closely aligned with the N-N axis (component along N-N: 8.64 D, in-plane component perpendicular to N-N: 0.38 D).

MNA crystallizes in the noncentrosymmetric monoclinic space group Ia (equivalent to Cc) with cell parameters $a=8.223(2)$ Å, $b=11.620(1)$ Å, $c=7.588(2)$ Å, $\beta=94.17(3)°$.

The choice of the Cartesian system in which the piezoelectric tensor d is to be expressed is usually dictated by symmetry considerations.[13] A Cartesian-coordinate system based on the molecular packing may be defined as follows. $\mathbf{E}_1$, parallel to $2\mathbf{a}+\mathbf{c}$, corresponds to the polar axis of the crystal. $\mathbf{E}_2$, parallel to $\mathbf{b}$, is the direction perpendicular to the mirror plane, while $\mathbf{E}_3$, in the mirror plane like $\mathbf{E}_1$, parallel to $-\mathbf{a}^*+2\mathbf{c}^*$, is perpendicular to the plane of all the molecules that are arranged in layers, the plane of each layer being perpendicular to $\mathbf{E}_3$ (Fig. 4).

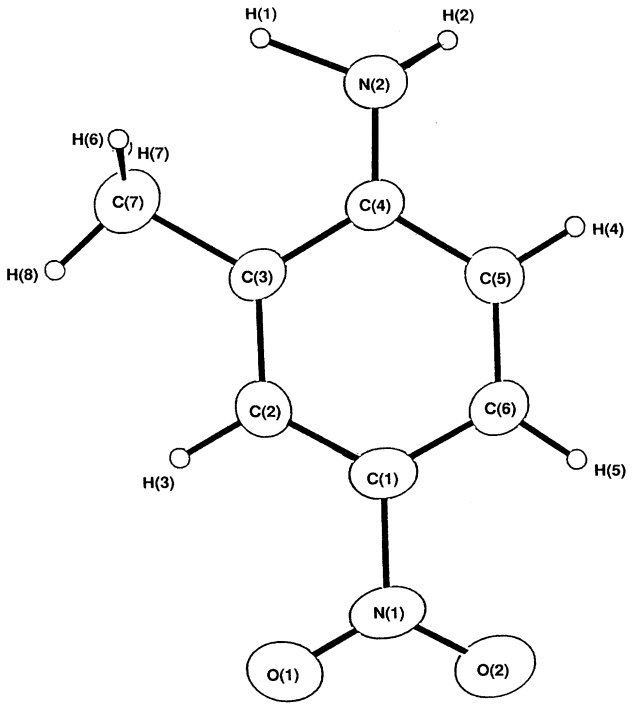

FIG. 3. The MNA molecule.

The distance between adjacent layers parallel to the $(\mathbf{E}_1,\mathbf{E}_2)$ plane is about 4 Å. The easy cleavage parallel to this plane gives evidence for the weakness of the interlayer interaction.

Within each layer, the centers of mass of neighboring molecules are separated by 8.802(2) Å and aligned exactly along the $\mathbf{E}_1$ direction. The main (N-N) axes of the molecules make angles of $\pm 19.5(2)°$ with this direction [Fig. 4(b)]. Because of the mirror symmetry, there is no net dipole-moment component along $\mathbf{E}_2$. Also, there is no component along the $\mathbf{E}_3$ direction, which is perpendicular to the plane of the benzene ring. $\mathbf{E}_1$ is therefore the unique polar direction, corresponding to a net dipole moment of about 30 D per unit cell. Successive molecules along $\mathbf{E}_1$ are linked by "head to tail" hydrogen bonding from the NH_2 group to the nitro group of the adjacent molecule.

$\Delta\theta$ measurements

To determine the piezoelectric tensor elements, the electric field was applied in the three perpendicular directions $\mathbf{E}_1$, $\mathbf{E}_2$, and $\mathbf{E}_3$. Details on the crystals and experimental conditions are given in Table I. In mounting the electrodes, great care was taken to minimize electric-field inhomogeneities and mechanical stress on the crystal. All measurements were made on four-circle Huber diffractometers with 2θ scans of 130 steps. In order to obtain high resolution in 2θ, a detector with a narrow slit (1 mm) was placed as far as possible from the crystal (1 m). Rotating anode and synchrotron sources were used in order to reach sufficient accuracy in $\Delta\theta$ in a reasonable amount of time. Each reflection measurement was repeated until a relative accuracy of at least 5σ in the θ shift was obtained.

A typical measurement is shown in Fig. 5(a). The difference curves $I_+ - I_0$ and $I_- - I_0$ clearly indicate the oppositely directed shifts, which are of the order of $10^{-3}°$. The same series of measurements with the field switched off are shown in Fig. 5(b). The lower part of Fig. 5(b) shows the statistical noise of the experiment.

Results

Verification of the Barsch equation

The variation of $\Delta\theta_{+0}$ and $\Delta\theta_{-0}$ as a function of the intensity of the field (reflection $-10\,0\,-4$ field along the polar axis) is shown in Fig. 6. The linearity of the dependence is as expected from expression (2). In Fig. 7, the $\Delta\theta_{+0}$ and $\Delta\theta_{-0}$ are plotted as a function of θ for all the reflections of the data set No. 1. The general trend is an increase of $\Delta\theta$ with θ, as predicted by the $\tan\theta$ term in the Barsch equation (broken line). This "$\tan\theta$" behavior is also shown in Fig. 8, where only the shifts of the $(0\,k\,0)$ reflections are plotted, the electric field being applied along the $\mathbf{E}_1$ direction (magnitude $E=5.0\times10^6$ V/m). In this particular case, the Barsch equation simplifies to $|\Delta\theta|=E|d_{12}|\tan\theta$.

By fitting the equation $\Delta\theta=a\tan\theta$ to the data, the piezoelectric element $|d_{12}|=2.6$ pC/N is readily de-

duced. This value is equal to the result of the full data set refinement, given below.

$\Delta\theta$ was found to be the same for Friedel-pair-related reflections, and independent of the frequency of the field (from 50 to 250 Hz).

The MNA piezoelectric tensor

The piezoelectric tensor in the point group m has ten independent nonzero elements:[14]

$$[d_{IJ}]=\begin{bmatrix} d_{11} & d_{12} & d_{13} & 0 & d_{15} & 0 \\ 0 & 0 & 0 & d_{24} & 0 & d_{26} \\ d_{31} & d_{32} & d_{33} & 0 & d_{35} & 0 \end{bmatrix},$$

where the abbreviated notation[14] has been used.

The piezoelectric-tensor elements are determined by least-squares from the measured $\Delta\theta$ values using the Barsch equation (2). Since each of the directions of the

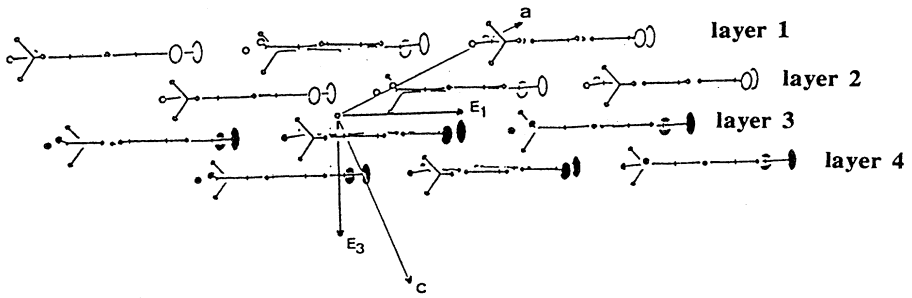

(a) View along E_2

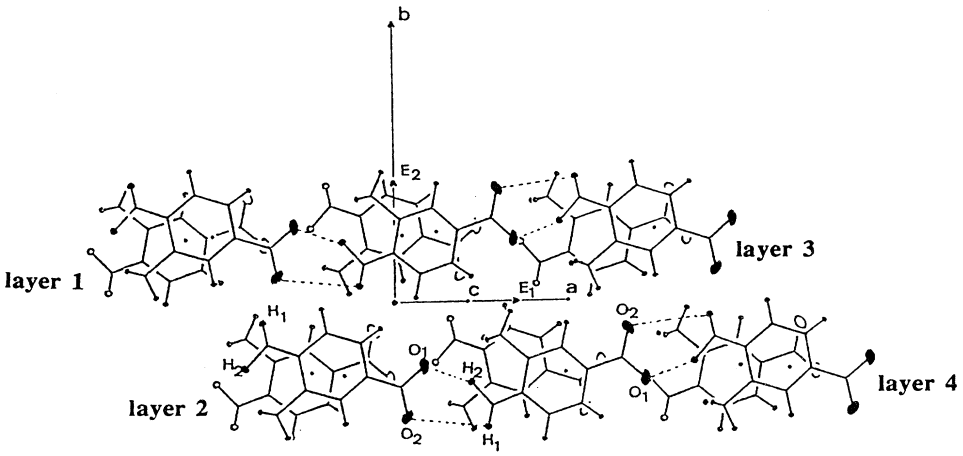

(b) View along E_3

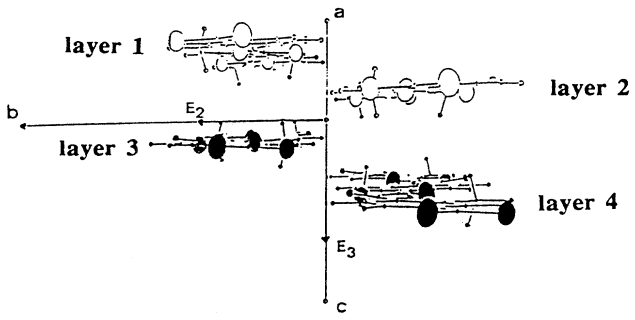

(c) View along E_1

FIG. 4. The MNA structure viewed along $\mathbf{E}_1$ (polar axis), $\mathbf{E}_2$ (**b** axis), and $\mathbf{E}_3$ (perpendicular to the plane of the molecules), respectively.

TABLE I. The MNA experiments.

	Data set No. 1	Data set No. 2	Data set No. 3
Crystal			
Dimensions (mm^3)	0.95/0.38/0.40	1.10/0.90/0.60	0.80/1.20/0.80
Growth	50% xylene 50% methanol evaporation	50% xylene 50% methanol evaporation	50% xylene 50% methanol evaporation
Data collection			
X-ray source	synchrotron (NSLS)	rotating anode	rotating anode
Wavelength Å	1.00	0.7107 (Mo $K\alpha$)	0.7107 (Mo $K\alpha$)
Temperature (°C)	≈20–25	≈20–25	≈20–25
Scan type	2θ	2θ	2θ
Number of unique reflections	56	9	13
Electric field			
Magnitude (10^6 V/m)	2.50	2.73	3.12
Direction	$\mathbf{E}_1 \| (2\mathbf{a}+\mathbf{c})$	$\mathbf{E}_2 \| \mathbf{b}$	$\mathbf{E}_3 \| (-\mathbf{a}^*+2\mathbf{c}^*)$
Frequency (Hz)	55–56	55–56	55–56

field corresponds to one of the Cartesian axes, each of the data sets gives information on one row of the tensor (No. $1 \rightarrow [d_{1J}]$, No. $2 \rightarrow [d_{2J}]$, No. $3 \rightarrow [d_{3J}]$). Since the absolute configuration of the crystal in the field is not known, the signs of the d_{IJ} remain undetermined. However, the *relative* signs within each row are correct, as the elements in one row originate from the same data set. The refinements are summarized in Table II. The results in the $\{\mathbf{E}_1\}$ coordinate system are

$$[d_{IJ}] = \begin{bmatrix} \delta_1 13.8(1) & \delta_1 2.5(1) & \delta_1 1.4(1) & 0 & \delta_1 5.3(3) & 0 \\ 0 & 0 & 0 & \delta_2 9.3(2) & 0 & \delta_2 5.1(2) \\ \delta_3 0.8(1) & -\delta_3 0.9(3) & \delta_3 2.4(2) & 0 & -\delta_3 2.5(7) & 0 \end{bmatrix} 10^{-12}\ \mathrm{C/N}\ , \tag{5}$$

where $\delta_i = \pm 1$.

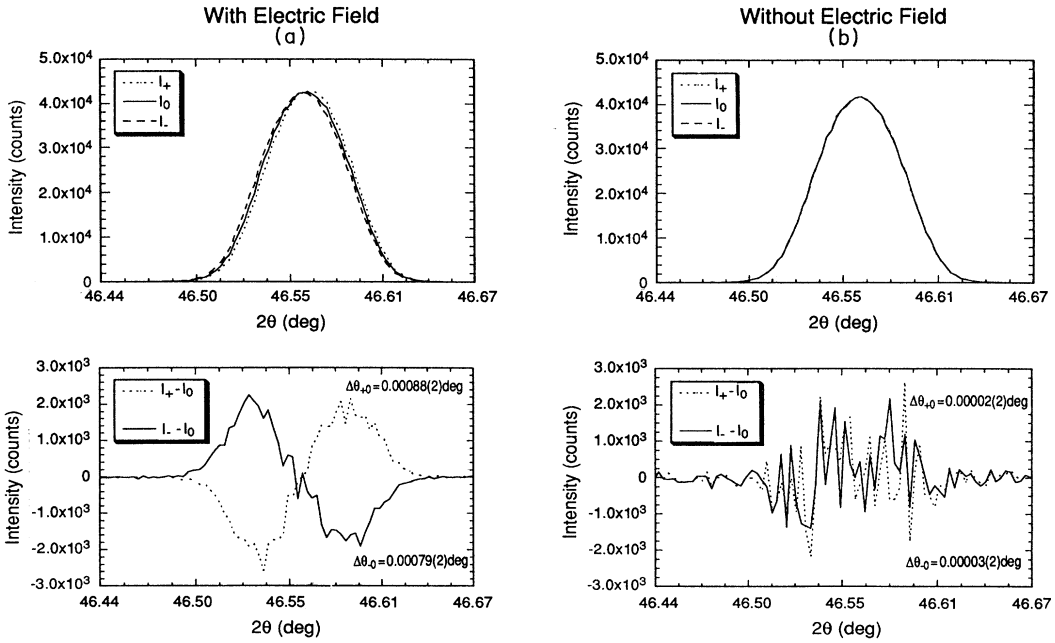

FIG. 5(a) The three profiles I_+, I_0, and I_- of the (6 0 2) reflection with electric field of magnitude 2.5×10^6 V/m applied along the polar axis. Below are plotted the differences $I_+ - I_0$ and $I_- - I_0$ with their standard deviations: the shift changes in sign as the field is reversed. (b) As (a), but without applied electric field. All three profiles are superimposed.

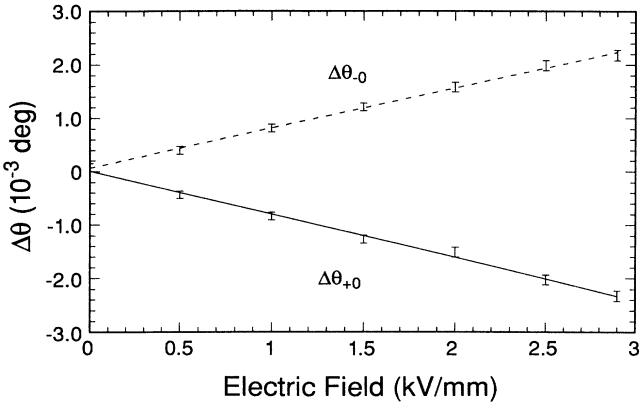

FIG. 6. $\Delta\theta_{+0}$ and $\Delta\theta_{-0}$ for the reflection (10 0 4) as function of an increasing electric field E applied along the polar axis. Error bars $\pm 1\sigma$.

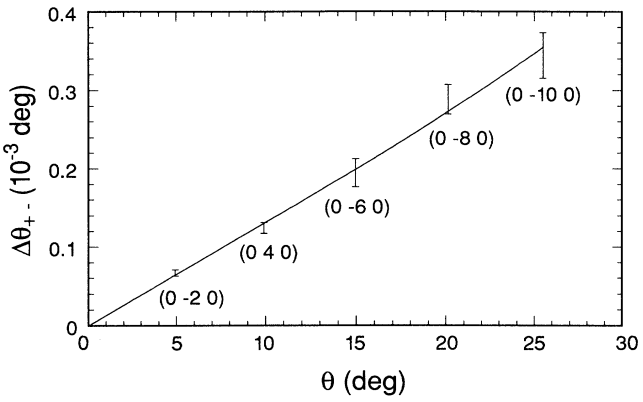

FIG. 8. θ shifts of the $(0\,k\,0)$ reflections compared with the predicted $\tan\theta$ dependence.

Strain tensors and cell deformations

For each applied electric field, the strain tensor ϵ_E (expressed in the Cartesian $\{\mathbf{E}_i\}$ system) can be readily deduced by substitution of (5) into expression (1). The ambiguity in the signs of the d_{IJ}'s is transferred to the signs of the rows in the strain tensor, but does not affect the calculated strain in any of the principal directions. For instance, the strains generated by a field in the $\mathbf{E}_I$ direction require only the elements $[d_{IJ}]$ and not those in the other rows of (5). The remaining uncertainty concerns the absolute signs of the ϵ_{ij}'s, or, in other words, the signs of the tensile and shear strains. This ambiguity would be resolved by the application of a field to a crystal cut in a general direction, which is experimentally difficult to achieve. It is of a somewhat limited practical interest, as the main response of the crystal occurs for fields parallel or perpendicular to the polar axis.

The translations $\{\mathbf{a}',\mathbf{b}',\mathbf{c}'\}$ of the deformed crystal can be computed from the strain-tensor elements and the zero-field values $\{\mathbf{a},\mathbf{b},\mathbf{c}\}$ using [15]

$$\begin{bmatrix}\mathbf{a}'\\ \mathbf{b}'\\ \mathbf{c}'\end{bmatrix}=(I+\epsilon_d)\begin{bmatrix}\mathbf{a}\\ \mathbf{b}\\ \mathbf{c}\end{bmatrix}, \tag{6}$$

where I is the identity matrix and ϵ_d is the strain tensor expressed in the crystal *direct* system $\{\mathbf{a},\mathbf{b},\mathbf{c}\}$. ϵ_d is readily deduced from ϵ_E through the mixed-tensor transformation

$$\epsilon_d = R\,\epsilon_{\mathrm{E}} R^{-1}, \tag{7}$$

where R is the transformation matrix from the Cartesian-coordinate system to the crystal system:

$$\begin{bmatrix}\mathbf{a}\\ \mathbf{b}\\ \mathbf{c}\end{bmatrix}=R\begin{bmatrix}\mathbf{E}_1\\ \mathbf{E}_2\\ \mathbf{E}_3\end{bmatrix}. \tag{8}$$

Since ϵ_E is a symmetrical tensor, it may also be referred to its principal axes $\{\mathbf{p}_i\}$, giving the diagonal tensor ϵ_{p}. The three mutually perpendicular directions $\{\mathbf{p}_i\}$ remain unchanged by the deformation. Table III gives the strain tensors ϵ_{E}, ϵ_{d}, and ϵ_{p} and the changes in the cell parameters for all three fields applied in this study.

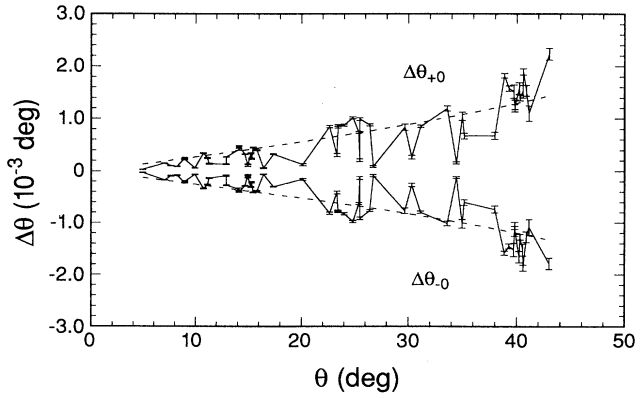

FIG. 7. $\Delta\theta_{+0}$ and $\Delta\theta_{-0}$ as function of θ for the electric field of 2.5×10^6 V/m applied along the polar axis. The broken lines represent a $\tan\theta$ dependence.

DISCUSSION

Orders of magnitude

The coefficient $d_{11}=\pm 13.8(1)$ pC/N is higher than the d_{IJ}'s of α quartz ($d_{11}=2.3$, $d_{14}=0.67$), but lower than the very large piezoelectric tensor elements of potassium dihydrogen phosphate (KDP) ($d_{36}=23.2$).[16] To our knowledge, this is the strongest piezoelectric behavior observed in an organic molecular crystal. It is larger than in benzil, for which d_{11} was measured as 10.7 pC/N.[17]

The strains induced by such a piezoelectric tensor are of the order of 10^{-5} for electric fields of 10^6 V/m, corresponding in the case of MNA, to changes in the cell dimensions of 10^{-4} Å and 10^{-3}°.

TABLE II. Refinement of the piezoelectric tensor elements.

Elements of the d_{IJ}	Number of parameters	Number of observations	$R(\Delta\theta^2)$ factor (%)	$R_w(\Delta\theta^2)$ factor (%)
$[d_{IJ}]$	4	56	5.8	5.6
$[d_{2J}]$	2	9	5.2	4.8
$[d_{3J}]$	4	13	5.3	5.3

Strains dominated by the polar direction

In order to illustrate the main piezoelectric effects, we shall retain only the largest d_{IJ}'s:[18]

$$d_E \approx \begin{bmatrix} d_{11} & 0 & 0 & 0 & 0 & 0 \\ 0 & 0 & 0 & d_{24} & 0 & 0 \\ 0 & 0 & 0 & 0 & 0 & 0 \end{bmatrix} . \quad (9)$$

Thus, for an electric field with three nonzero components E_1, E_2, and E_3, the induced strain tensor ϵ_E is

$$\epsilon_E(E_1E_2E_3) \approx \begin{bmatrix} d_{11}E_1 & 0 & 0 \\ 0 & 0 & \frac{d_{24}}{2}E_2 \\ 0 & \frac{d_{24}}{2}E_2 & 0 \end{bmatrix} , \quad (10)$$

which leads to the following conclusions. (i) The main tensile strain ϵ_{11} is a contraction (or expansion) along the polar axis, and can only be induced by an electric field applied along this polar axis. (ii) The main shear strain ϵ_{23} is perpendicular to the polar axis, and can only be in-

TABLE III. Strains tensors (in 10^{-5}) as a function of electric-field direction. ϵ_E, ϵ_d, and ϵ_p are the strain tensors expressed in the Cartesian $\{\mathbf{E}_i\}$ (see text for the definition), direct $\{\mathbf{a}_i\}$, and principal-axes $\{\mathbf{p}_i\}$ systems, respectively; δ_1, δ_2, and δ_3 stand for "±."

$\mathbf{E}_1 \| (2\mathbf{a}+\mathbf{c})\delta_1$ $E_1 = 2.50\times10^6$ V/m	$\mathbf{E}_2 \| \mathbf{b}\delta_2$ $E_2 = 2.73\times10^6$ V/m	$\mathbf{E}_3 \| (-\mathbf{a}^*+2\mathbf{c}^*)\delta_3$ $E_3 = 3.12\times10^6$ V/m
$\epsilon_E =$		
$\begin{bmatrix} 3.45(3) & 0 & 0.60(4) \\ 0 & 0.63(4) & 0 \\ 0.60(4) & 0 & 0.35(3) \end{bmatrix}$	$\begin{bmatrix} 0 & 0.69(2) & 0 \\ 0.69(2) & 0 & 1.26(3) \\ 0 & 1.26(3) & 0 \end{bmatrix}$	$\begin{bmatrix} 0.25(2) & 0 & 0.39(3) \\ 0 & 0.28(3) & 0 \\ 0.39(3) & 0 & 0.74(2) \end{bmatrix}$
$\epsilon_d =$		
$\begin{bmatrix} 2.53(4) & 0 & 1.38(3) \\ 0 & 0.63(4) & 0 \\ 1.72(3) & 0 & 1.27(3) \end{bmatrix}$	$\begin{bmatrix} 0 & 0.26(3) & 0 \\ 0.06(4) & 0 & 0.93(2) \\ 0 & 2.19(4) & 0 \end{bmatrix}$	$\begin{bmatrix} 0.61(3) & 0 & 0.42(3) \\ 0 & 0.28(3) & 0 \\ 0.47(3) & 0 & 0.38(3) \end{bmatrix}$
$\epsilon_p =$		
$\begin{bmatrix} 3.56 & 0 & 0 \\ 0 & 0.63 & 0 \\ 0 & 0 & 0.24 \end{bmatrix}$	$\begin{bmatrix} 1.43 & 0 & 0 \\ 0 & 0.00 & 0 \\ 0 & 0 & 1.43 \end{bmatrix}$	$\begin{bmatrix} 0.96 & 0 & 0 \\ 0 & 0.04 & 0 \\ 0 & 0 & 0.28 \end{bmatrix}$
Principal axes:		
$\mathbf{p}_1 \|$ $0.98\mathbf{E}_1+0.18\mathbf{E}_3$	$0.34\mathbf{E}_1+0.71\mathbf{E}_2+0.62\mathbf{E}_3$	$-0.48\mathbf{E}_1+0.88\mathbf{E}_3$
$\mathbf{p}_2 \|$ $\mathbf{E}_2$	$-0.88\mathbf{E}_1+0.48\mathbf{E}_3$	$0.88\mathbf{E}_1+0.48\mathbf{E}_3$
$\mathbf{p}_3 \|$ $-0.18\mathbf{E}_1+0.98\mathbf{E}_3$	$0.34\mathbf{E}_1-0.71\mathbf{E}_2+0.62\mathbf{E}_3$	$\mathbf{E}_2$
Changes in the cell parameters:		
Δa (10^{-4} Å)=1.98(3)	0	0.53(2)
Δb (10^{-4} Å)=0.73(5)	0	0.32(3)
Δc (10^{-4} Å)=0.88(3)	0	0.32(2)
$\Delta\alpha$ (10^{-3}°)=0	0.63(4)	0
$\Delta\beta$ (10^{-3}°)=1.76(4)	0	0.51(3)
$\Delta\gamma$(10^{-3}°)=0	0.09(3)	0
$\Delta a/a$(10^{-5})=2.41(4)	0	0.64(3)
$\Delta b/b$(10^{-5})=0.63(4)	0	0.28(3)
$\Delta c/c$(10^{-5})=1.16(3)	0	0.42(3)
$\Delta\alpha/\alpha$ (10^{-5})=0	1.81(4)	0
$\Delta\beta/\beta$ (10^{-5})=1.87(4)	0	0.54(3)
$\Delta\gamma/\gamma$ (10^{-5})=0	0.10(3)	0

duced by a field along the **b** axis. (iii) A field applied along the $\mathbf{E}_3$ axis (i.e., perpendicular to the plane of the molecules) has no significant effect.

It should be mentioned that a slightly larger value of ϵ_E can be obtained by applying the field along the direction $\mathbf{p}_1 = 0.98\mathbf{E}_1 + 0.18\mathbf{E}_3$ (see Table III), which makes an angle of 10.6° with the polar axis (see Fig. 8). This direction is nearly parallel to the principal optical axis of MNA, which is inclined at 8(1)° to the polar axis.[8]

External strain versus internal strain

The deformation of a crystal may be considered as a superposition of a pure lattice (external) strain and of an internal strain.[19,20] The former keeps the atomic fractional coordinates constant, changing only the unit-cell geometry, whereas the latter has the opposite effect. In the case of a molecular crystal like MNA, the external strain would correspond to intramolecular deformations, as if the unit-cell medium was deformed continuously in a rubberlike manner. The internal strain can then be considered as a relaxation of the crystal structure in order to respond to these energetically unfavorable displacements.[21]

From the measurements of the shifts in the Bragg angles, only the external displacements can be deduced. But the internal displacements (i.e., the changes in the fractional coordinates) are accessible from the measurements of the variations in the diffracted intensities. The total displacement can be determined by combining the two sets of measurements.

Piezoelectric and electro-optic effects

In view of our new results, we reconsider the interpretation of the large electrooptic effect in MNA given by Lipscomb, Garito, and Narang.[8]

The linear electro-optic (LEO) effect is defined as the change in the optical permittivity ϵ^{-1} (and thus the refractive indices **n**) of the crystal induced by an applied electric field **E**:[22]

$$\Delta\left[\frac{1}{n_{ij}^2}\right] = \sum_{k=1}^{3} r_{ijk} E_k \ , \tag{11}$$

where the r_{ijk}'s are the electro-optic coefficients.

The LEO effect arises from the coupling interaction of two electric fields with matter: the optical field $\mathbf{E}_{\text{optical}}$, and the applied field $\mathbf{E}_{\text{LF}}$, usually static or of low frequency (<1 MHz). $\mathbf{E}_{\text{optical}}$ modifies the refractive index through a *direct* (nonlinear) interaction with the molecular electron density. But there is also a possible *indirect* LEO effect, which is more subtle: first, E_{LF} modifies the vibrations of the lattice (acoustic phonons), which, in turn, influence the optical response of the molecules through the phonon-electron interaction. In macroscopic terms, $\mathbf{E}_{\text{LF}}$ induces an elastic deformation of the crystal via the *piezoelectric* effect, which modifies the refractive index via the *elasto-optic* (or *photoelastic,* or *piezo-optic*) effect. The total LEO effect is the sum of both the direct and indirect effects:

$$\mathbf{r} = \mathbf{r}^{\text{electronic}} + \mathbf{r}^{\text{electron-phonon}} \ .$$

The contribution of the electronic states to the LEO coefficients can be determined experimentally by comparing the LEO susceptibility χ^{LEO}, and the second-harmonic generation susceptibility χ^{SHG} of only electronic origin.[23]

In their measurement of the LEO effect in MNA, Lipscomb, Garito, and Narang[8] applied a static electric field of about 10^6 V/m along the X and Z principal optical axes, which are nearly parallel to the $\mathbf{E}_1$ and $\mathbf{E}_3$ directions defined above. The χ^{LEO}_{111} susceptibility was derived from the measured r_{111} value as $(540\pm100)\times10^{-12}$ m/V, while χ^{SHG}_{111} (calculated from the reported second-harmonic coefficient d_{111}) was found to be $(500\pm125)\times10^{-12}$ m/V. Notwithstanding the large uncertainties, Lipscomb, Garito, and Narang[8] concluded that "the large value of the linear electro-optic effect in MNA is predominantly electronic in nature," the electron-phonon coupling (i.e., the piezoelectric-photoelastic effect) being negligible. The large piezoelectric coefficients of MNA obtained in our work indicate the importance of the low-frequency contributions, and are at variance with this interpretation. Indeed, 2-methyl-4-nitro-N-methylaniline (MNMA), very similar to MNA, has LEO coefficients known to be dominated by the electrically induced strains.[24]

CONCLUDING REMARKS

We conclude that x-ray diffraction can be used to determine the piezoelectric tensors of small crystals. The determination of the response at the atomic level requires analysis of the very small intensity changes which accompany the shift in the reflection positions. Preliminary results of such studies on MNA have been reported.[5] With a few exceptions,[25,26] the microscopic theory of piezoelectricity has received little attention. Experimental data on atomic and molecular displacements in crystals subjected to external fields can now be obtained with the techniques described above.

ACKNOWLEDGMENTS

Support of this work by the National Science Foundation (Grant No. CHE8711736) is gratefully acknowledged. The SUNY X3 beamline is supported by the Division of Basic Energy Sciences of the U.S. Department of Energy (Grant No. DEFG0286ER45231). The National Synchrotron Light Source, Brookhaven National Laboratory is supported by the U.S. Department of Energy, Division of Materials Sciences and Division of Chemical Sciences.

APPENDIX: THE DERIVATIVE METHOD FOR CALCULATION OF THE PROFILE SHIFTS

Using the modulation method with the 2θ scan mode, three profiles $I_0, I_\pm$ of N points each are collected simultaneously. Assuming the variation of the intensity at each point to be due to the shifts $\Delta 2\theta_{\pm 0}$ of the profiles $I_\pm$

relative to the profile I_0, the intensity $I_+(2\theta_i)$ [or $I_-(2\theta_i)$] at each point of the profile is given by

$$I_\pm(2\theta_i)\approx I_0(2\theta_i-\Delta 2\theta_{\pm 0,i}) , \quad \text{(A1)}$$

where $\Delta 2\theta_{\pm 0,i}$ is the shift of the profile I_+ (or I_-) at point i of the scan.

As $\Delta 2\theta_{\pm 0,i}$ is very small, $I_0(2\theta_i-\Delta 2\theta_{\pm 0,i})$ may be developed to first order in $\Delta 2\theta_{\pm 0,i}$:

$$I_0(2\theta_i-\Delta 2\theta_{\pm 0,i})\approx I_0(2\theta_i)-\dot{I}_0(2\theta_i)\Delta 2\theta_{\pm 0,i} , \quad \text{(A2)}$$

where

$$\dot{I}_0(2\theta_i)=\left[\frac{\partial I_0}{\partial 2\theta}\right]_{2\theta=2\theta_i} , \quad \text{(A3)}$$

which gives for the intensity difference $\Delta I_{\pm 0}=I_\pm-I_0$

$$\Delta I_{\pm 0}(2\theta_i)=-\dot{I}_0(2\theta_i)\Delta 2\theta_{\pm 0,i} . \quad \text{(A4)}$$

In terms of local-response ratios, $\eta_{\pm 0,i}=\Delta I_{\pm 0}(2\theta_i)/I_0(2\theta_i)$, the shift in 2θ at each point of the profile is equal to

$$\Delta 2\theta_{\pm 0,i}=-\eta_{\pm 0,i}\frac{I_0(2\theta_i)}{\dot{I}_0(2\theta_i)} . \quad \text{(A5)}$$

*Present address: Laboratoire de Cristallographie, CNRS, 25 avenue des Martyrs, 38000 Grenoble, France.
†Authors to whom correspondence should be addressed.
‡Permanent address: Synchrotron Radiation Research Center, No. 1 R&D Road VI, Hsinchu Science-Based Industrial Park, Hsinchu 30077, Taiwan, Republic of China.

[1]G. R. Barsch, Acta Crystallogr. Sec. A **32**, 575 (1976).
[2]A. Paturle, H. Graafsma, J. Boviatsis, A. Legrand, R. Restori, P. Coppens, Å. Kvick, and R. Wing, Acta Crystallogr. Sec. A **45**, FC25 (1989).
[3]L. Godefroy (unpublished).
[4]I. Fujimoto, Acta Crystallogr. Sec. A **38**, 337 (1982).
[5]H. Graafsma, A. Paturle, and P. Coppens, *Systematic Study of the Effect of an Electric Field on the X-ray Scattering Intensity of Organic Crystals,* ACA Abstracts, Series II (AIP, New York, 1990), p. 57.
[6]B. F. Levine, C. G. Bethea, C. D. Thurmond, R. T. Lynch, and J. L. Bernstein, J. Appl. Phys. **50**, 2523 (1979).
[7]H. Itoh, K. Hotta, H. Takara, and K. Sasaki, Appl. Opt. **25**, 1491 (1986).
[8]G. F. Lipscomb, A. F. Garito, and R. S. Narang, J. Chem. Phys. **75**, 1509 (1981).
[9]Y. Tokura, A. Kurita, and T. Koda, Phys. Rev. B **31**, 2588 (1985).
[10]Y. Kubota and T. Yoshimura, Appl. Phys. Lett. **53**, 2579 (1988).
[11]D. K. Deshpande, M. A. Shashidbar, and R. K. Suryanarayana, Z. Phys. Chem. (Leipzig) **262**, 588 (1981).
[12]M. Dupuis, J. Rys, and H. F. King, J. Chem. Phys. **65**, 111 (1976).
[13]Proc. IRE **37**, 1378 (1949).
[14]J. F. Nye, *Physical Properties of Crystals,* 1st ed. (Clarendon, Oxford, 1957).
[15]A. Paturle, Ph.D. thesis, University of Grenoble, France, 1990.
[16]*Crystal and Solid State Physics, Zahlenwerte und Funktionen aus Naturwissenschaften und Technik,* edited by K. H. Hellwege, Landolt-Börnstein, New Series, Group III, Vol. 2 (Springer-Verlag, Berlin, 1969).
[17]S. Haussuhl, Acta Crystallogr. **23**, 666 (1967).
[18]We consider only the d_{IJ}'s greater than 4 pC/N, keeping in mind that the d_{IJ} with $J=4,5,6$ are half their values in the uncontracted tensor.
[19]M. Born and K. Huang, *Dynamical Theory of Crystal Lattices* (Oxford University, New York, 1954), p. 134.
[20]M. Catti, Acta Crystallogr. Sec. A **45**, 20 (1989).
[21]T. H. K. Barron, T. G. Gibbons, and R. W. Munn, J. Phys. C **4**, 2805 (1971).
[22]D. S. Chemla and J. Zyss, *Nonlinear Optical Properties of Organic Molecules and Crystals* (Academic, New York, 1987), Chaps. 2–8.
[23]M. Sigelle and R. Hierle, J. Appl. Phys. **52**, 4199 (1981).
[24]K. Sutter, C. Bosshard, M. Ehrensperger, P. Gunter, and R. J. Twieg, IEEE J. Quantum Electron. **QE-24**, 2362 (1988).
[25]H. Kaplan, in *Proceedings of the International Conference on Lattice Dynamics, Copenhagen, Denmark, 1963,* edited by R. F. Wallis (Pergamon, Oxford, 1963).
[26]A. G. McLellan, J. Phys. C **17**, 2999 (1984).